NASA/TM—2006-214445 AIAA–2006–4010

Aerosol-Assisted Chemical Vapor Deposited Thin Films for Space Photovoltaics

Aloysius F. Hepp, Jeremiah S. McNatt, and John E. Dickman
Glenn Research Center, Cleveland, Ohio

Michael H.-C. Jin
University of Texas at Arlington, Arlington, Texas

Kulbinder K. Banger and Christopher V. Kelly
Ohio Aerospace Institute, Brook Park, Ohio

Angel R. Aquino González and Angus A. Rockett
University of Illinois, Urbana, Illinois

November 2006

NASA STI Program . . . in Profile

Since its founding, NASA has been dedicated to the advancement of aeronautics and space science. The NASA Scientific and Technical Information (STI) program plays a key part in helping NASA maintain this important role.

The NASA STI Program operates under the auspices of the Agency Chief Information Officer. It collects, organizes, provides for archiving, and disseminates NASA's STI. The NASA STI program provides access to the NASA Aeronautics and Space Database and its public interface, the NASA Technical Reports Server, thus providing one of the largest collections of aeronautical and space science STI in the world. Results are published in both non-NASA channels and by NASA in the NASA STI Report Series, which includes the following report types:

- TECHNICAL PUBLICATION. Reports of completed research or a major significant phase of research that present the results of NASA programs and include extensive data or theoretical analysis. Includes compilations of significant scientific and technical data and information deemed to be of continuing reference value. NASA counterpart of peer-reviewed formal professional papers but has less stringent limitations on manuscript length and extent of graphic presentations.

- TECHNICAL MEMORANDUM. Scientific and technical findings that are preliminary or of specialized interest, e.g., quick release reports, working papers, and bibliographies that contain minimal annotation. Does not contain extensive analysis.

- CONTRACTOR REPORT. Scientific and technical findings by NASA-sponsored contractors and grantees.

- CONFERENCE PUBLICATION. Collected papers from scientific and technical conferences, symposia, seminars, or other meetings sponsored or cosponsored by NASA.

- SPECIAL PUBLICATION. Scientific, technical, or historical information from NASA programs, projects, and missions, often concerned with subjects having substantial public interest.

- TECHNICAL TRANSLATION. English-language translations of foreign scientific and technical material pertinent to NASA's mission.

Specialized services also include creating custom thesauri, building customized databases, organizing and publishing research results.

For more information about the NASA STI program, see the following:

- Access the NASA STI program home page at *http://www.sti.nasa.gov*

- E-mail your question via the Internet to *help@sti.nasa.gov*

- Fax your question to the NASA STI Help Desk at 301–621–0134

- Telephone the NASA STI Help Desk at 301–621–0390

- Write to:
  NASA STI Help Desk
  NASA Center for AeroSpace Information
  7121 Standard Drive
  Hanover, MD 21076–1320

NASA/TM—2006-214445 AIAA–2006–4010

Aerosol-Assisted Chemical Vapor Deposited Thin Films for Space Photovoltaics

Aloysius F. Hepp, Jeremiah S. McNatt, and John E. Dickman
Glenn Research Center, Cleveland, Ohio

Michael H.-C. Jin
University of Texas at Arlington, Arlington, Texas

Kulbinder K. Banger and Christopher V. Kelly
Ohio Aerospace Institute, Brook Park, Ohio

Angel R. Aquino González and Angus A. Rockett
University of Illinois, Urbana, Illinois

Prepared for the
Fourth International Energy Conversion Engineering Conference and Exhibit (IECEC)
sponsored by the American Institute of Aeronautics and Astronautics
San Diego, California, June 26–29, 2006

National Aeronautics and
Space Administration

Glenn Research Center
Cleveland, Ohio 44135

November 2006

Acknowledgments

The authors gratefully acknowledge NASA for financial support cooperative agreement NCC3–947 and NCC04AA71A. We also wish to thank Mr. David Scheiman from the Ohio Aerospace Institute for his assistance with the solar simulator at NASA Glenn Research Center and Mr. Philip Jenkins also from the Ohio Aerospace Institute for his assistance with the *PL* measurements. We are grateful to Dr. Robert Birkmire, Dr. William Shafarman, and the staff at the Institute of Energy Conversion of the University of Delaware for their help with solar cell fabrication. We also acknowledge the contributions of Dr. Jerry Harris from Northwest Nazarene University, Dr. William Buhro and Dr. Jennifer Hollingsworth from Washington University, Dr. John Scofield from Oberlin College, and Mr. Jonathan Cowen from Case Western Reserve University. Finally, we acknowledge Dr. Kannan Ramanathan of NREL for providing a shadow mask.

Level of Review: This material has been technically reviewed by technical management.

Available from

NASA Center for Aerospace Information
7121 Standard Drive
Hanover, MD 21076–1320

National Technical Information Service
5285 Port Royal Road
Springfield, VA 22161

Available electronically at http://gltrs.grc.nasa.gov

Aerosol-Assisted Chemical Vapor Deposited Thin Films for Space Photovoltaics

Aloysius F. Hepp, Jeremiah S. McNatt, and John E. Dickman
National Aeronautics and Space Administration
Glenn Research Center
Cleveland, Ohio 44135

Michael H.-C. Jin
University of Texas at Arlington
Arlington, Texas 76019

Kulbinder K. Banger and Christopher V. Kelly
Ohio Aerospace Institute
Brook Park, Ohio 44142

Angel R. Aquino González and Angus A. Rockett
University of Illinois
Urbana, Illinois 61801

Abstract

Copper indium disulfide thin films were deposited via aerosol-assisted chemical vapor deposition using single source precursors. Processing and post-processing parameters were varied in order to modify morphology, stoichiometry, crystallography, electrical properties, and optical properties in order to optimize device-quality material. Growth at atmospheric pressure in a horizontal hot-wall reactor at 395 °C yielded best device films. Placing the susceptor closer to the evaporation zone and flowing a more precursor-rich carrier gas through the reactor yielded shinier, smoother, denser-looking films. Growth of (112)-oriented films yielded more Cu-rich films with fewer secondary phases than growth of (204)/(220)-oriented films. Post-deposition sulfur-vapor annealing enhanced stoichiometry and crystallinity of the films. Photoluminescence studies revealed four major emission bands (1.45, 1.43, 1.37, and 1.32 eV) and a broad band associated with deep defects. The highest device efficiency for an aerosol-assisted chemical vapor deposited cell was 1.03 percent.

Nomenclature

*AM*0	air mass zero (space solar spectrum)
*AM*1.5	air mass one point five (solar spectrum at sea level)
CIGS	copper indium gallium diselenide ($CuIn_{1-x}Ga_xSe_2$ - a I-III-VI_2 material)
(AA)CVD	(aerosol-assisted) chemical vapor deposition
DAP	donor-acceptor pair
EDS	energy dispersive spectroscopy
FF	fill factor
J_{sc}	short-circuit current
η	solar cell efficiency
PL	photoluminescence
SEM	scanning electron microscopy
SSP	single-source precursor(s)
V_{oc}	open-circuit voltage
(GA)XRD	(glancing angle) X-ray diffraction

I. Introduction

The development of new technologies that will enable the exploration of the universe has been one of the major goals of the National Aeronautics and Space Administration (NASA) since its founding in 1958. Technologies that will enable the design of new spacecraft, rovers, satellites, and other space vehicles will assist the agency in its quest

to explore and understand planetary systems, stars, and finally the universe. As part of its efforts to fulfill these goals, NASA GRC has been working on the deposition and fabrication of lightweight, thin film solar cells for space power (refs. 1 to 9). The ability to deposit thin films on lightweight, flexible polymer substrates will lead to more design flexibility, lower launch costs, and extra space and mass for payloads.

Depositing high quality absorber layers on polymer substrates has been a challenge because polymer substrates do not withstand the high deposition temperatures used in standard deposition processes. Temperatures below 400 °C are usually needed to ensure that the polymer substrate does not suffer thermal degradation. Because of this temperature constraint, copper indium disulfide ($CuInS_2$) was deposited using single-source precursors (SSPs) with low decomposition temperatures (<250 °C) that were synthesized in-house (refs. 1 to 5). Films were deposited using an aerosol-assisted chemical vapor deposition (*AACVD*) reactor to exploit the lower deposition temperature enabled by the simpler decomposition chemistry resulting from the presence of all of the essential elements in the SSPs (refs. 6, 7, and 9). *AACVD* is a simple and inexpensive process that offers the advantage of a uniform, large-area deposition, just like metal organic CVD, while also offering the low-temperature solution reservoir typical of spray pyrolysis methods.

Polycrystalline $CuInS_2$ was chosen as the absorber layer because of its high absorption coefficient and its direct band gap of 1.5 eV, which is near optimum for *AM*0 conditions. So far, the highest total area efficiency achieved by a $CuInS_2$ cell using co-evaporation techniques has been 12.5 percent (ref. 10). Other alloys of $Cu(In,Ga)(S,Se)_2$, such as $Cu(In,Ga)Se_2$ (*CIGS*), have shown conversion efficiencies as high as 19.2 percent under *AM*1.5 illumination (ref. 11); but the 1.5 eV direct band gap of $CuInS_2$ makes it ideal for solar radiation conversion in space. Polycrystalline devices typically outperform single crystal devices created under similar conditions (ref. 12). Furthermore, polycrystalline films can be deposited on a broader range of substrates, including polymers, and are less sensitive to deposition conditions. $CuInS_2$ thin films are also more resistant to radiation in space than other *CIGS* alloys (refs. 13 and 14); they can be used as a top cell in a tandem structure with *CIGS* (ref. 15); and they are less toxic to process than selenium-containing alloys.

*SSP*s have the I-III-VI_2 stoichiometry "built in" and offer a clean approach for depositing thin films. One advantage is that they offer a number of tunable sites within the complex, allowing various combinations for depositing chalcopyrite films of different compositions. The structure of an *SSP* is shown in figure 1. Early work was performed by Nomura (refs. 16 to 19) and Kanatzidis (ref. 20). Buhro and Hepp later demonstrated that $(PPh_3)_2Cu(SEt)_2In(SEt)_2$ could be used in a spray *CVD* process for depositing $CuInS_2$ thin films under 400 °C (refs. 21 to 23). Prior to our efforts, very few ternary *SSP*s were known, characterized, and used in thin film deposition; Hepp and Banger have made numerous findings on the synthesis and use of *SSP*s. A review of this work was recently reported (ref. 3).

Throughout the studies performed at NASA GRC, various processing and post-processing parameters were modified in order to determine how these affected morphology, stoichiometry, crystallography, electrical properties, and optical properties of deposited thin films. Some of the modifications made included varying the reactor type and configuration, deposition temperatures, location of the substrate within the reactor, annealing times, and annealing atmospheres. This review will discuss several deposition setups, details of processing experiments, and their impact on film properties. A number of characterization techniques including X-ray diffraction (XRD), scanning electron microscopy (*SEM*), and photoluminescence (*PL*) were used to obtain film properties. Complete working devices were also fabricated and tested.

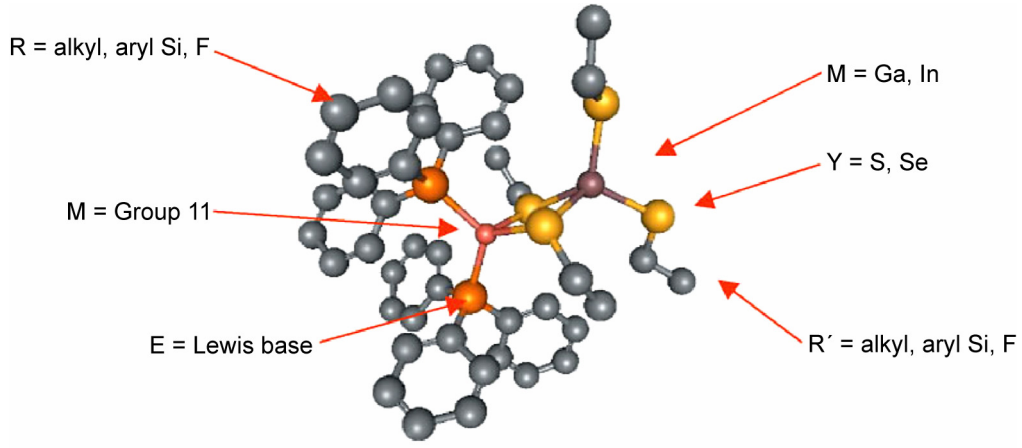

Figure 1.—Structure of [{PPh3}2Cu(SEt)2In(SEt)2], indicating tunable sites.

II. Experimental

A. Reactor Designs

Three different reactors were used to deposit $CuInS_2$ films via *AACVD*; the first reactor design discussed was primarily used in our parametric study. This reactor was a horizontal atmospheric pressure hot-wall reactor (reactor A, fig. 2(a)) with a plate-type 2.5 MHz ultrasonic nebulizer from Sonaer Ultrasonics. The precursor (1.5 to 3.5 g) was dissolved into distilled toluene (50 to 400 ml) and fed into the nebulizer using a syringe pump. This nebulizer created an aerosol that was swept into the reactor by an Ar carrier gas at a flow rate of 4 l/min (or SLPM). The reactor is a two-zone furnace consisting of a warm precursor evaporation zone and a hot deposition zone. The aerosol is converted to precursor vapor and mixes with the reactor gas in the evaporation zone. A solid graphite susceptor coated with SiC was placed in the deposition zone.

The second reactor was a vertical atmospheric pressure, cold-wall reactor (reactor B, fig. 2(b)) with a commercial ultrasonic nozzle (Sono-Tek 120 kHz); the third reactor was a horizontal low-pressure hot-wall reactor (reactor C) with a pulsed aerosol injection system using a commercial automotive fuel-injector (Ford 2M2EA7B). Most depositions were done on 0.87 by 7.6 by 0.1 cm soda lime glass slide substrates (Fisher 12-550 A) coated with Mo using a radio-frequency magnetron sputtering system.

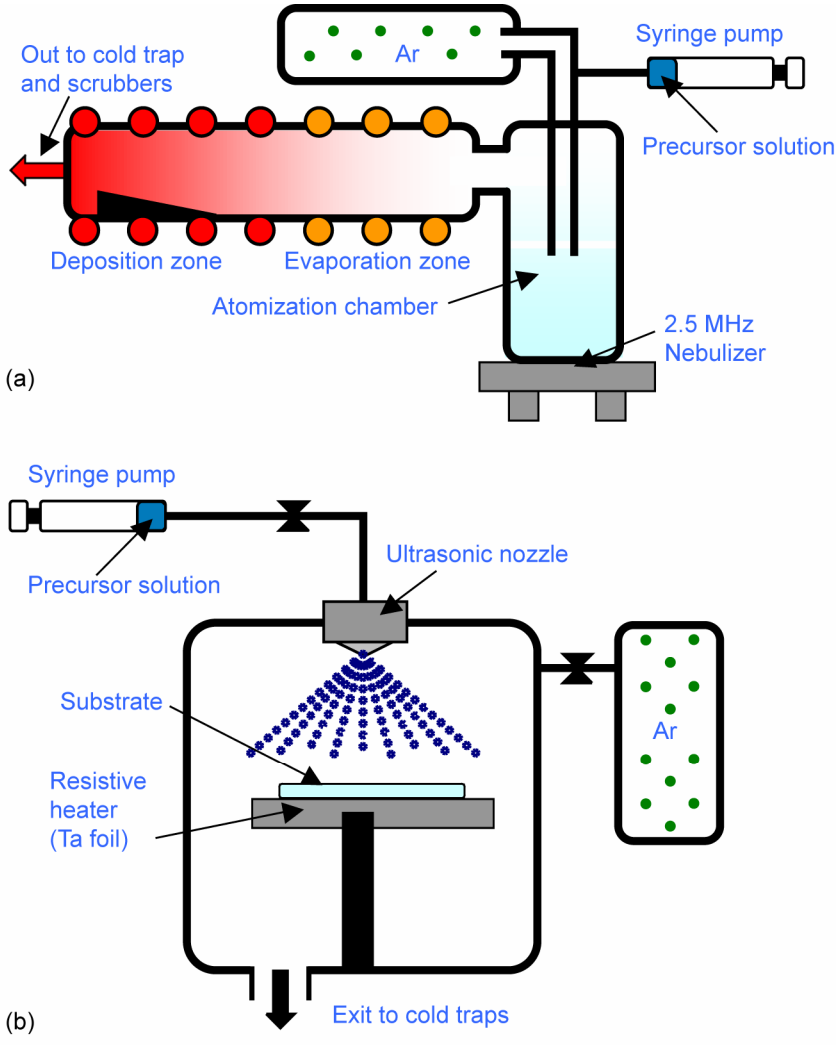

Figure 2.—Schematic of two of the reactors used in part II.A: (a) atmospheric pressure horizontal hot-wall reactor (Reactor A) and (b) the vertical cold-wall reactor (Reactor B).

Even though all three reactors share the same precursor delivery system (*AACVD*), each tool offers specific advantages. For example, a cold wall reactor (reactor B) will help prevent decomposition of the precursor before it reaches the substrate. A pulsed aerosol injection system at low pressure (reactor C) will allow the film to grow under better-defined conditions than in a continuous process because of the minimization of undesirable transient effects due to the high volatility of the solvents used (ref. 24). A more detailed description of each of the conditions for film growth, including reactor type, precursor type, delivery method, deposition temperatures, growth time, and other parameters are summarized in table I. Depositions were done on bare and Mo-coated glass slides from Corning (Corning 2947 and 7059). Commercial Mo foil substrates were also used. Post-deposition annealing of film III was performed in a tube furnace (Lindberg 54477) at 600 °C for 10 min under N_2 flow (4 SLPM).

TABLE I.—GROWTH PARAMETERS FOR *AACVD* DEPOSITED $CuInS_2$ FILMS

Film	I	II	III	IV	V
Reactor	A		B	C	
Precursor	Solid		Liquid		
Precursor concentration (M)	0.01				
Precursor delivery method	Carrier gas			Vacuum-driven	
Precursor delivery rate (ml/min)	~1.7		1.5	0.4	
Temperatures (°C) Evaporation zone: Deposition zone: Substrate:	 128 390 390[#]	 120 360 360[#]	 no zones 400	 250 250 420	 150 250 400
Pressure (torr)	atm.			~12	~10
Ar flow rate (l/min)	4			0.08[*]	0.15[*]
Substrate	Mo/glass (corning 2947)	Mo foil	Glass (corning 7059)	Mo/glass (corning 2947)	
Substrate size (cm by cm by 0.1 cm)	0.87 by 7.6		2.5 by 2.5	2.5 by 7.6	
Growth time (min)	80	60		250	
Thickness (μm)	~1		~4	~1	

Solid precursor: $(PPh_3)_2CuIn(SEt)_4$
Liquid precursor: $\{P(n\text{-}Bu)_3\}_2CuIn(SEt)_4$
[#]Substrate is located within the deposition zone.
[*]Direct reading from MKS flow controller (not calibrated). Ar flow is required for the aerosol creation mechanism.

B. Conditions Used for Atmospheric Pressure Hot-Wall Reactor Parametric Study

The reactor used for this study was the horizontal atmospheric-pressure hot-wall reactor (reactor A). The susceptor accommodated three substrates side by side at an angle of 15.5° above horizontal. The leading edge of the film experiences a more reactant-rich gas stream and is closer to the bottom of the reactor. The environment of the trailing edge, deeper in the deposition zone, is more product-rich and is closer to the axial center of the reactor tube.

In order to optimize thin film and device quality, a four-phase study was conducted. The temperature of the deposition zone, location of the susceptor along the length of the reactor tube, concentration of the precursor solution, and post-deposition annealing conditions were varied individually. Initially, the substrate temperature was varied between 350 and 425 °C. In the second phase, the measured distance from the end of the reactor tube up to the trailing edge of the susceptor were varied from 57.15 mm (2.25 in.) to 127 mm (5 in.). The larger the distance, the closer to the evaporation warm zone. For phase three, the precursor concentration was varied between 0.005 and 0.04 mol/l. The deposition temperatures for the two middle parts of the experiment were maintained at a fixed value of 395 °C. Finally, post-deposition annealing of films was performed in the reactor. The evaporation zone temperature was set to 120 °C and run-to-run deposition zone temperatures were varied between 450 and 580 °C. During annealing, Ar was flowed through the reactor tube at a rate of 10 ml/min. Annealing times varied from 15 min to 17 hr. The annealing times began when the annealing temperature was reached and ended when the cooling process started. It took about 30 min to reach the annealing temperature when started at room temperature and a little over 1 hr to cool down to room temperature. For some runs, sulfur vapor was added during annealing by placing sulfur (Strem Chemicals, 99+ percent) in a powder-filled crucible in the evaporation zone.

C. Fabrication of $CuInS_2$ Solar Cells

Complete $CuInS_2$ solar cells were fabricated at GRC; the cell architecture is shown in figure 3. After coating the glass substrates with Mo, $CuInS_2$ films were deposited via *AACVD*, following procedures optimized for the

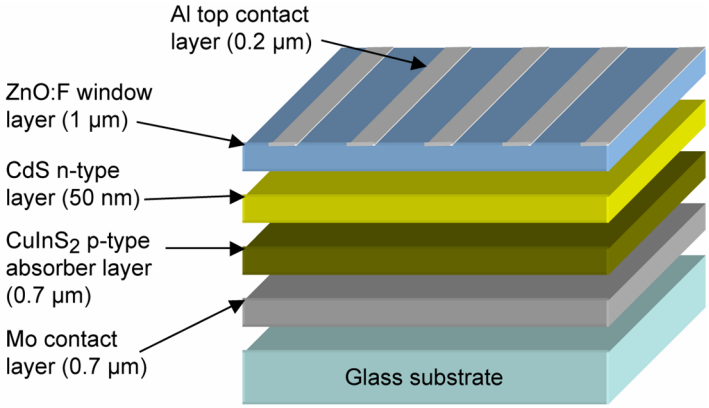

Figure 3.—Schematic of standard NASA GRC thin-film $CuInS_2$ solar cell architecture.

atmospheric-pressure hot-wall reactor (reactor A). Post-deposition, sulfur/Ar-anneals were performed from 450 to 580 °C for up to 17 hr. The films were then etched in a 1.5 M KCN solution for 1 min at room temperature to remove residual Cu_2S. Cadmium sulfide (CdS) was then deposited on the films using chemical bath deposition (CBD) to form the collecting heterojunction. The CBD used a solution of 0.001 M $CdSO_4$, 1.5 M NH_4OH, and 0.0075 M thiourea ($H_2NC(S)NH_2$). The bath was heated to 70 °C. Samples were immersed into the bath for 7 to 10 min until the solution started turning yellow. Once the CdS had been deposited, films were placed in an ultrasonic bath to remove particulates. A layer of ZnO:F was deposited from a 16.5 cm (6.5 in.) diameter F-doped ZnO target in a RF sputtering system using pure Ar as the sputter gas. Aluminum (Al) was used as the top contact metal. A 0.2 μm thick layer of Al was deposited by thermal evaporation through a shadow mask. The devices were isolated by mechanically scribing. The final cell area of the GRC-produced devices was typically ~0.4 cm^2.

Solar cells were also fabricated at the Institute for Energy Conversion (IEC) following their well-established fabrication process (ref. 25). This was done in order to isolate issues related to *AACVD* deposition of CIS films from those associated with the rest of the solar cell fabrication at GRC. For the cells prepared at IEC, only CIS layers were deposited at GRC. The rest of the device fabrication, including the coating of the glass substrates with Mo and the mechanical scribing, were performed at IEC. Final cell area for IEC-produced devices was typically ~0.45 cm^2. Finally, post-fabrication anneals were carried out in air on a hot plate (Cimarec 2) at 150 °C for up to 24 hr.

D. Characterization Techniques

Following growth of films and completion of devices, characterization techniques were employed to determine the properties and performances of the films and devices. Film thicknesses were measured using a profiler (Sloan Dektak IIA or KLA-Tencor HRP 75). Film morphologies were studied using *SEM* (Hitachi S-3000N and S-800). The Hitachi S-3000N includes a built-in *EDS* (EDAX, Falcon) system used to examine film compositions. Compositional measurements were performed in different areas across each cell in order to determine the compositional uniformity. The Cu/In ratios were obtained by quantifying the Cu K and In L emission lines using the ZAF standardless method. XRD (PANalytical X'pert Pro) was used in order to identify the phases and glancing angle X-ray diffraction (*GAXRD*) was performed using the same instrument in order to identify the phases present at the film surfaces. The optical bandgaps of the films were determined by analyzing transmittance measurements taken in a UV/VIS spectrophotometer (Perkin-Elmer Lamda-19). Electrical measurements were performed using a four-point probe system (Bio-Rad HL5500PC) operated in the van der Pauw configuration and a custom hot-point probe system—a commercial soldering iron (Weller TC201) was used as the hot probe.

Films annealed at 450 °C for 7 hr were characterized using photoluminescence (*PL*). It has been previously shown that annealing can remove structural defects associated with metal ions in films, thereby improving the electronic properties of the absorber layer (refs. 26 and 27). $CuInS_2$ films were excited using an Ar ion laser system (Coherent Innova 70) with an excitation wavelength of 514 nm. In order to control the laser power density, neutral density filters were used. The *PL* emission detection system consisted of a liquid nitrogen-cooled charge-coupled device (CCD) (Horiba Jobin Yvon, Symphony), a germanium detector (EG&G Judson, J16D), and a lock-in system (Stanford Research System, SR810DSP). The detectors were connected to a Spex 1269 monochromator, while the samples were mounted on a helium cryostat (Janis, STVP-100) in order to lower the temperature to 4 K. Finally, devices were tested using a solar simulator at GRC (Spectrolab X-25 Mark II) to obtain current versus voltage curves under *AM*0 illumination. Calibration was performed using a standard GaAs single-junction solar cell.

III. Results and Discussion

A. Impact of Reactor Design

In an initial precursor decomposition study, three different reactors were used to grow $CuInS_2$ films. Hot-wall reactors (A (film I) and C (films IV and V)) produced dense, columnar grain growth while the cold-wall reactor (film B (III)) yielded porous nanostructures. This can be clearly seen in the *SEM* micrographs in figure 4, for films I, III, IV, and V (see table I for deposition conditions). Figure 4(a), the cross-sectional image of film I, shows a columnar grain structure. The columnar grain structure lowers the cross section for photo-excited carrier recombination at grain boundaries, thus improving the performance of the solar cells.

Figure 4(b) shows a plan-view image of film III together with an inset of the same region at a higher magnification. Under low magnification, only the round structures appeared; however, when the magnification was increased smaller nanoparticles (~100 nm) were seen. The nanoparticles may have been created above the hot substrate by pyrolysis of nano-droplets generated from the aerosol (ref. 28). Under this model, the ultrasonically excited aerosol continues to flow through until it breaks into numerous nano-droplets. Other proposed models include nanoparticles coagulating before landing on the growth surface (ref. 29), and liquid deposition taking place instead of vapor deposition due to the partial evaporation of the liquid droplet (ref. 30).

Film IV can be seen in figure 4(c). It exhibits a dendritic microstructure with non-faceted, elongated grains. It was previously proven that this was a consequence of diffusion-limited growth (ref. 21). By increasing the flow rate, dense and trigonal-shaped faceted grains were obtained for film V (fig. 4(d)). This shape is due to the intersection of {211} faces in the chalcopyrite structure. The largest grain sizes obtained using *SSP*s were of the order of 0.5 μm for film V.

XRD patterns revealed that the films were either (112) or (204/220) oriented. Differentiation between the chalcopyrite and sphalerite phases was made by differences in XRD patterns (ref. 31). XRD patterns for all five films can be seen in figure 5(a). It was found that films often contained a secondary phase ($2\theta = 26.5°$), believed to be indium-rich (In-rich) (ref. 7). The more the film was In-rich, the more likely it was that the secondary phase was present with the film being more (204/220)-oriented. *EDS* measurements (not shown) indicate that the films containing the secondary phase were In-rich and that the Cu/In ratio increased when the secondary phase was reduced upon annealing (fig. 5(b)). In order to confirm the In-rich nature of the secondary phase, *GAXRD* was performed on the films. The *GAXRD* pattern (fig. 5(c)) revealed that the secondary phase was concentrated at the surface. In order to find out the chemical nature of the phase, films containing the phase were etched in a 10 percent aqueous KCN solution for 2 min. It is common to etch Cu-rich $CuInS_2$ films in this solution prior to CdS deposition to remove undesired CuS_x compounds segregated on the surface during $CuInS_2$ deposition. In addition, it is also known that the etch rate of Cu-rich compounds in KCN solutions is much higher than In-rich compounds (ref. 33). After etching, *GAXRD* still showed the presence of the secondary phase on the surface without any change in its diffraction intensity, meaning that the phase is not CuS_x. The nature of the secondary In-rich phase was also confirmed by Raman spectroscopy (ref. 7).

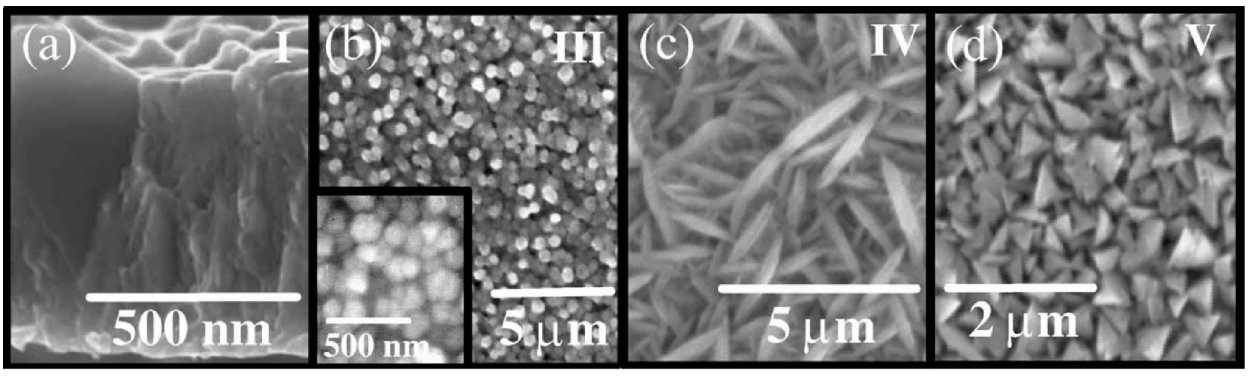

Figure 4.—SEM micrographs of AACVD grown $CuInS_2$ thin films: (a) cross-sectional image of film I, (b) plane-view image of film III (inset at higher magnification), (c) plane-view image of film IV, and (d) plane-view image of film V.

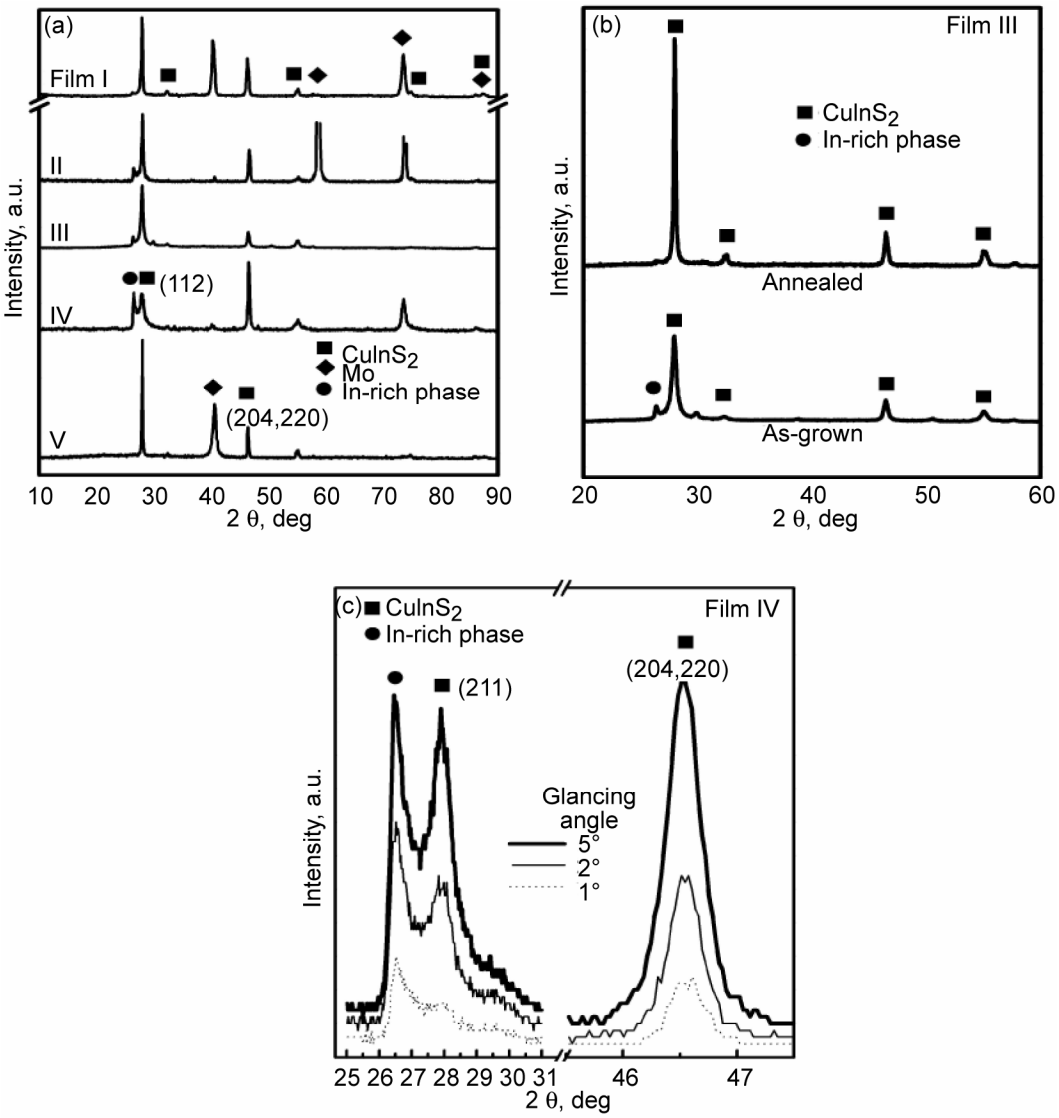

Figure 5.—XRD spectra of CuInS2 films grown by AACVD: (a) untreated films, (b) film III with post-deposition annealing, and (c) GAXRD spectrum of film IV.

One way to prevent the formation of the secondary phase is to favor growth conditions of (112)-oriented films and avoid the surface kinetic regime where (204/220)-oriented film is favored. In our setup, for any reactor, the substrate temperature had to stay around 400 °C in order to promote the growth of (112)-oriented films without a high concentration of the In-rich secondary phase. Attempts to grow (204/220)-oriented films without the secondary phase were not successful. Another way to reduce this secondary phase is by post-deposition heat treatment.

Bandgap energies between 1.45 and 1.47 eV were obtained for the films. The band gap energies were estimated using plots of $(\alpha h\nu)^2$ versus E (fig. 6), where α is an absorption coefficient estimated from optical transmittance data and hν is the photon energy. Figure 6 shows that the band edge sharpens upon post-growth annealing, which is ascribed to improved crystallinity and densification (film III). The overall absorption of film V was higher than that of film III in the figure, and this could be attributed to the difference in the density between the two films; film V had a denser grain structure than film III as shown in figure 4. This could be attributed in part to differences in reflectivity; this will be better defined by further work.

All of the films grown showed p-type conduction regardless of the reactor type, Cu/In ratio, or morphology. It was reported that S-rich material shows p-type conduction (refs. 33 and 34); and that the Cu-on-In antisite (Cu_{In}) in Cu-rich films is expected to be the major acceptor for p-type conduction (ref. 35). The bulk resistivities ranged from 0.1 to 30 Ω-cm; Cu-rich films generally had lower resistivity than In-rich films.

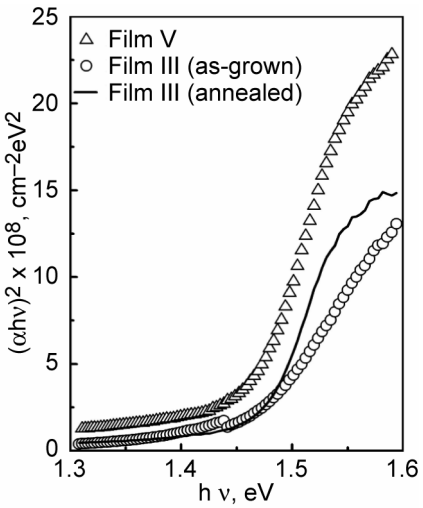

Figure 6.—Plot of $(\alpha h\nu)^2$ vs. *E* for films III and V.

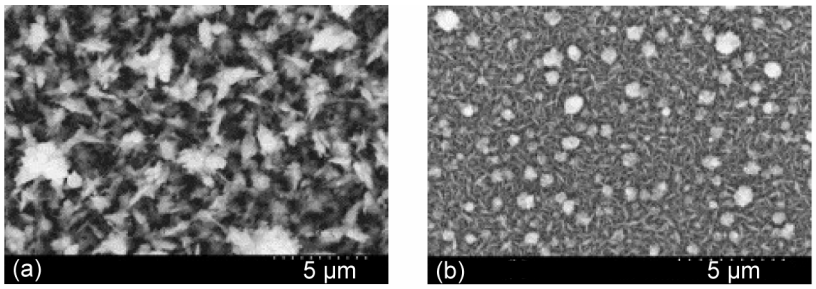

Figure 7.—SEM images of $CuInS_2$ films grown by AACVD: (a) porous, rough, dull films, and (b) smooth, shiny, dense films.

B. Atmospheric Pressure Hot-Wall Reactor Parametric Study

As discussed above, in this experiment various reactor parameters were manipulated in order to study their effects on film growth. In general, the leading edge of the films tended to be smooth, shiny, and dense, while the trailing edge tended to be rough, dull, and highly porous. The rough surface morphology can be attributed to the stronger diffusion-limited film growth at the trailing edge (ref. 36). By the time the carrier gas (Ar) reaches the trailing edge of the substrate, it may be less precursor-rich than the gas flowing over the leading edge – reaction occurs on the hot wall of the reactor along the deposition zone. This would make the concentration boundary layer thicker at the trailing edge of the substrate, requiring the precursor to diffuse a greater distance to reach the surface of the trailing edge and hence the film growth would be more diffusion-limited. *SEM* images of a rough, dull film can be seen below in figure 7(a); the images of a smooth, shiny film can be seen in figure 7(b).

Run to run deposition zone temperature (350 to 425 °C) was the first parameter varied. Temperature variation affected film stoichiometry (fig. 8(a)) and crystalline orientation (fig. 8(b)) while not significantly affecting the deposition rate (fig. 8(c)). From figure 8(a), we can see that the films were closest to stoichiometry when deposited at 395 °C. Cu-to-In ratios ranged from 0.79 to 0.98, with the highest ratio occurring also at 395 °C. The higher deposition zone temperature correlated to increased sulfur content in the films. The crystalline structure was also affected by deposition zone temperature.

$CuInS_2$ films deposited in this study were observed to be crystallographically (220/204)-oriented or (112)-oriented by XRD. Chalcopyrite solar cells had a higher series resistance for the (220/204)-oriented films (ref. 37). From XRD measurements in figure 8(b), we observed that deposition temperatures around 395 °C yielded higher ratios of the preferred (112)-oriented films. Finally, deposition rates were not limited by supply of thermal energy (temperature variation), therefore film growth was not reaction-limited, see figure 8(c).

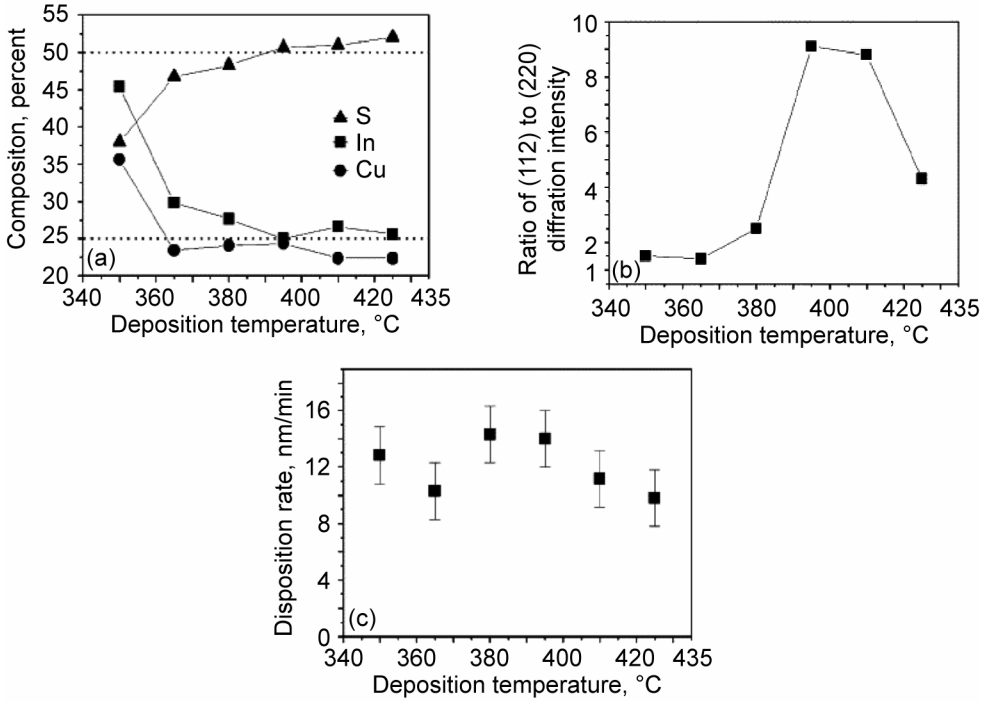

Figure 8.—Deposition temperature vs. (a) elemental composition, (b) crystalline orientation, and (c) deposition rate for $CuInS_2$ films with precursor feed rate of 1.6 g/h.

The next parameter varied was the location of the susceptor within the deposition zone. Variations of the susceptor location did not affect film stoichiometry, but they did influence the morphologies of the films. When the susceptor was moved towards the evaporation zone, denser and smoother, shiny looking films were obtained due to a reduced concentration boundary layer (less diffusion-limited) towards the evaporation zone.

The single-source precursor concentration in the carrier solvent was another of the parameters varied. The concentrations of the *SSP* in toluene were varied between 0.005 to 0.04 mol/l. There were no significant changes in elemental composition of the films as a function of concentration, but increasing the precursor concentrations gave smoother, shinier films than with lower concentrations. This is due to the fact that at higher precursor concentrations, more precursor compound was available to the film, reducing the effects of a diffusion limited growth process.

The final parameter manipulated was post-deposition annealing. It was determined that post-deposition annealing improves the elemental composition and crystalline structure of films. For example, after a 5 hr anneal at 580 °C in a sulfur-rich atmosphere, typical film elemental compositions changed from 51.5 percent S, 24.5 percent In, and 24.0 percent Cu, to 52.0 percent S, 23.5 percent In, and 24.5 percent Cu. Annealing increased the Cu-to-In ratio which is correlated with improved electrical properties for $CuInS_2$ films (ref. 38). Another advantage of annealing in a S-rich atmosphere is that increased S content passivates S vacancies, an undesirable n-type dopant (ref. 39). Ordering of the Cu and In atoms within the crystalline structure also increased, producing a better ordered chalcopyrite film. $CuInS_2$ films typically occur in either a sphalerite (more disordered) or a chalcopyrite structure. Evidence of a more ordered chalcopyrite structure can be seen in figure 9, where the (101) and (211) diffractions at 17.9° and 37.3°, respectively, can be clearly seen in the annealed film. Another characteristic of the chalcopyrite structure not seen in the sphalerite structure is the peak splitting in the (200)/(004) and (116)/(312) diffractions at 32.2/32.4° and 54.8/55.1°, respectively. The highest efficiency for a cell made with a *AACVD*-deposited film using *SSP*s was 1.0 percent and the film was annealed under S/Ar at 450 °C for about 7 hr (ref. 8). The highest efficiency for a cell made with a non-annealed film was 0.9 percent (ref. 8). Both cells had smooth, shiny, and dense $CuInS_2$ absorber layers.

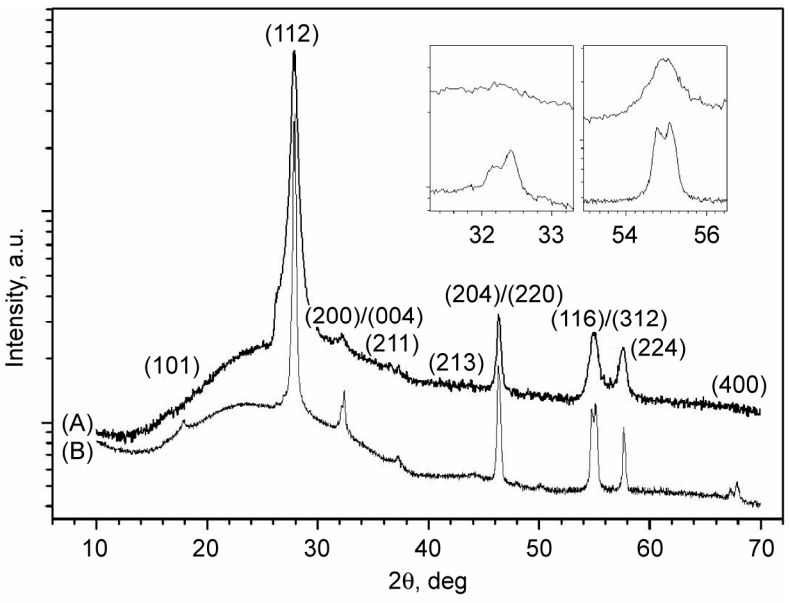

Figure 9.—XRD pattern from (A) as deposited films and (B) annealed film.

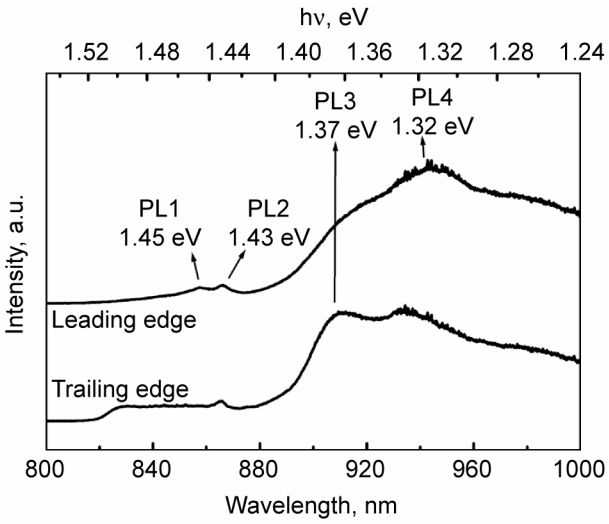

Figure 10.—Photoluminescence spectra of as-deposited $CuInS_2$ thin films made from a SSP.

C. Post-Deposition Annealing Effects Studied by Photoluminescence

PL measurements were performed on 76 mm (3 in.) long annealed films grown by the process used in the previous experiment. *PL* spectra of the leading and trailing edges were recorded for as-deposited, S-annealed, and Ar-annealed films. As mentioned in previous sections, the leading edges were always more In-rich than the trailing edges and, therefore have lower Cu-to-In ratios (0.84 compared to the 1.03). Four different emission bands - *PL*1 at 1.45 eV, *PL*2 at 1.43 eV, *PL*3 at 1.37 eV, and *PL*4 at 1.32 eV in figure 10 were identified in both the leading and trailing edges of almost all samples (*PL*1 was not clearly seen in some samples). For the as-deposited films, a near band-edge emission can be seen for the trailing edge sample in figure 10. This is probably due to the combination of excitonic recombination and other transitions associated with unidentified shallow defect levels (ref. 27). Clear differences between the leading and trailing edges were observed from emission bands associated with deeper defect levels. For the trailing edges, the intensities of *PL*3 at 1.37 eV were always higher than those of *PL*4 at 1.32 eV (fig. 10). Finally, the broad, deep-level emission bands spanning from 1.32 to 1.24 eV actually tailed down to 0.9 eV, as measured by a Ge detector.

After post-deposition Ar and Ar/S-annealing, the films were studied again using *PL*. S-anneals reduced the relative intensities of the *PL*1, *PL*4, and broad emission bands, while Ar-anneals increased the relative intensity of the *PL*1 band. This can be seen in figure 11. We can also see in this figure that S-anneals suppressed the broad near band-edge emission from the trailing edge samples. When *EDS* measurements were performed on the films after S-anneals, an extra 1 to 2 at percent S was found incorporated into the films. On the other hand, when Ar-anneals were performed, a 5 to 6 at percent S loss occurred. XRD measurements yielded the same results as above, where more ordered chalcopyrite structures were obtained after S-anneals (ref.8). S-anneals yielded higher resistivity films while Ar-anneals yielded lower resistivity films. Hot-probe measurements showed that all annealed films showed p-type conduction.

The excitation intensity was also varied in order to determine the effect it had on the *PL* spectrum. *PL*1 and *PL*3 bands had a blueshift per decade of 3.7 and 5.5 meV, respectively, with an increase in excitation intensity. The blueshifts were attributed to donor-acceptor pair (*DAP*) recombination (refs. 27 and 40). *PL*2 did not show any excitation power dependency, while the analysis of the *PL*4 band was not attempted because of the uncertainty in its precise location. The effect of increasing excitation intensity can be clearly seen in figure 12.

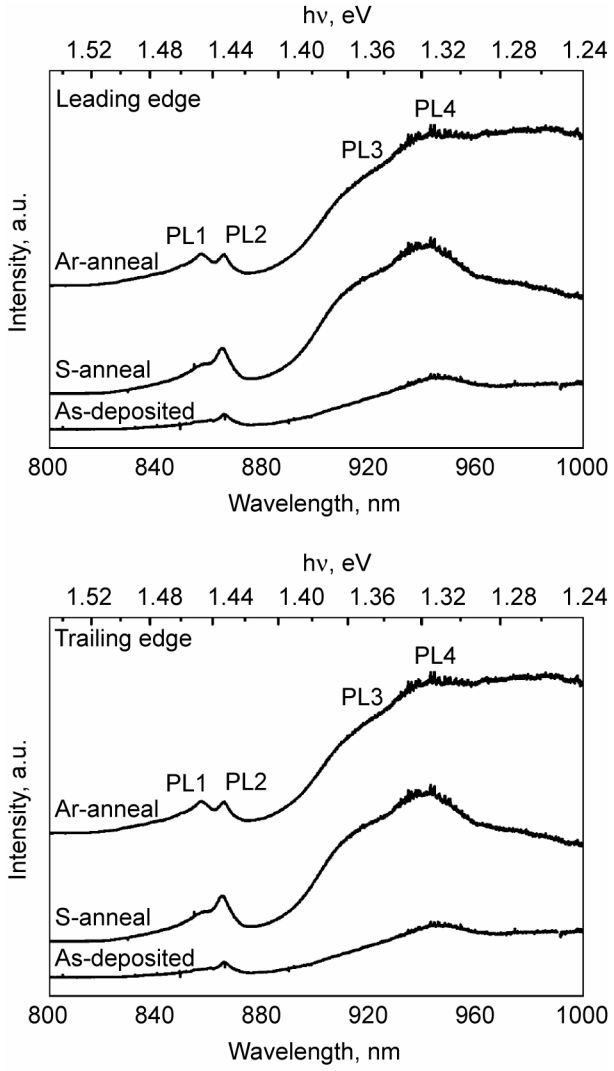

Figure 11.—Photoluminescence spectra of $CuInS_2$ films prior to annealing and after annealing in either S/Ar or Ar flow at 450 °C for 7 hours.

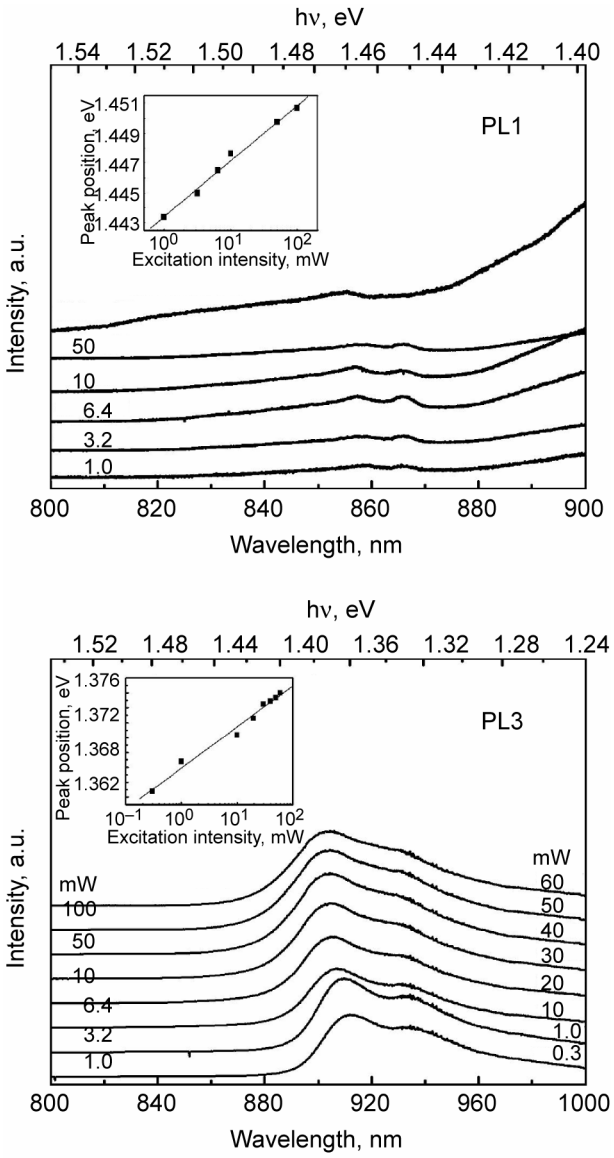

Figure 12.—Spectra of $CuInS_2$ films with various excitation intensities; the insert shows the blueshift of PL1 (top) and PL3 (bottom) emission bands.

The blue shift of the bands with increasing excitation intensity is explained as follows. The emission energy for the recombination can be given by:

$$h\nu(r) = E_g - (E_A + E_D) + \frac{e^2}{\varepsilon r_{DA}} \tag{1}$$

where E_g is the band gap, E_A (E_D) is the activation energy of the acceptor (donor), and $e^2/\varepsilon r_{DA}$ is the Coulomb energy for the pair at a distance r_{DA} (ref. 40). When the excitation energy increases, the film is flooded with photo-generated carriers. As a result, the average separation between the donor and the acceptor decreases causing the blueshift.

Shallow donors and acceptors for $CuInS_2$ have been previously studied and identified (refs. 39 and 41 to 45). Figure 13 includes some of the most energetically favorable intrinsic defects used in our analysis to assign transitions to the four different emission bands. Shallow donors include: sulfur vacancy (V_S), In-on-Cu antisite (In_{Cu}), and indium interstitial (I_i). Acceptors include: copper vacancy (V_{Cu}), Cu-on-In antisite (Cu_{In}), and copper

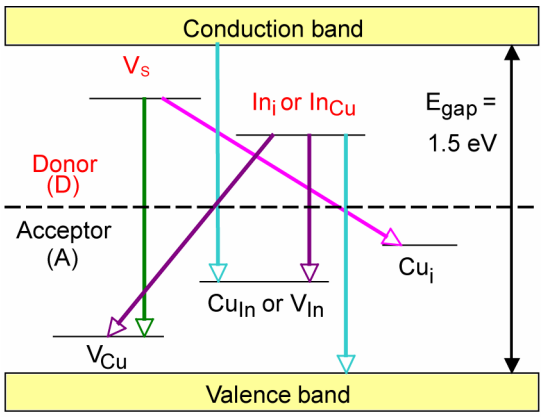

PL Band	Energy (eV)	Transition (D-A)
PL1	1.45	V_S - V_{Cu}
PL2	1.43	In_{Cu} /In_i – VB or CB – Cu_{In}/V_{In}
PL3	1.37	In_{Cu} /In_i – V_{Cu} /Cu_{In}/V_{In}
PL4	1.32	V_S-Cu_i

Figure 13.—Diagram and table of tentative assignment of transitions for the different PL bands.

interstitial (Cu_i). The *PL*1 emission band at 1.45 eV was assigned to a donor-acceptor transition, because of its blueshift upon increasing excitation intensity. V_S was attributed to the donor state because of the band's sensitivity to the change of V_S concentration upon annealing, and V_{Cu} was attributed to the acceptor state because the *PL*1 intensity was relatively stronger in leading edge (In-rich) samples. The *PL*2 band at 1.43 eV was assigned to a defect-band transition because there was no noticeable blueshift with increasing excitation energy. The *PL*3 band at 1.37 eV was assigned to transitions between metal ions (refs. 39 and 46). Finally, the *PL*4 band at 1.32 eV was assigned to a V_S-Cu_i transition. When the film was S-annealed, this band was suppressed; S incorporates into the structure reducing the V_S concentration (ref. 46).

D. Testing of CIS Solar Cells

The best cell fabricated at GRC was made from a film deposited using a 0.01 M solution. After deposition, a S-anneal at 450 °C for 17 hr was performed. This cell was not annealed after fabrication. The Mo bottom contact layer had a sheet resistance of 0.5 Ω/sq and a thickness of 0.7 μm. The CdS layer had an optical transmittance of 65 percent at a photon energy of 1.5 eV. GRC-fabricated cells used a 1 μm thick, n-type ZnO:F window layer with a sheet resistance of 200 Ω/sq and a transmittance of 85 percent at a photon energy of 1.5 eV. Thickness of Al top contact was ~200 nm. The characteristic curve for this cell together with cell parameters can be found in figure 14 and table II, respectively.

The cell fabricated at IEC is also included in figure 14 and table II. This cell was fabricated from a film deposited using a 0.04 M solution and S-annealed at 450 °C for 6 hr and 40 min. The completed cell was then annealed under air at 150 °C for about 24 hr. This cell's window layer, a 70 nm thick i-ZnO layer, had a transmittance of over 90 percent at a photon energy of 1.5 eV. The sheet resistance of the double top contact layer (2 μm Al/50 nm Ni) was about 1.8 Ω/sq. Both cells had nearly the same efficiency (~1 percent), but the IEC cell had a higher shunt resistance, which improved the fill factor (table II). The use of the intrinsic ZnO and the Ni/Al top contact improved the quality of the IEC cells by lowering the series resistance and improving the fill factor, as previously reported in the literature (ref. 15). It should be also noted that most solar cells prepared with the *AACVD* method in the literature had a superstrate structure (ref. 6); there has been no report of a working device with a typical chalcopyrite solar cell structure (top contact/window layer/CdS/$CuInS_2$/Mo/ substrate) except for the authors' previous results (ref. 47).

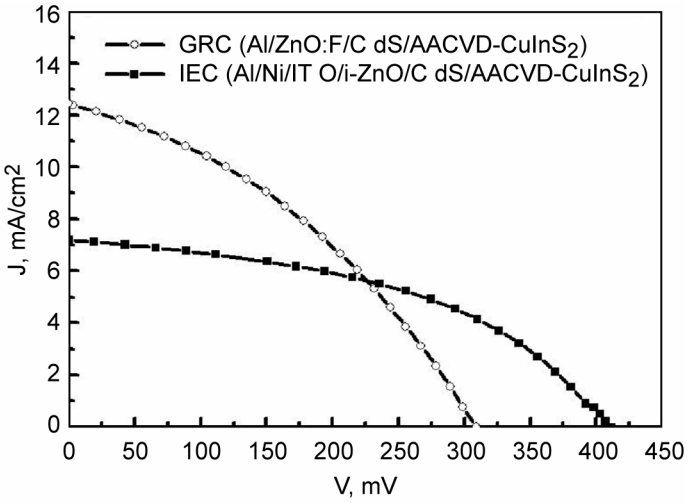

Figure 14.—Light J-V characteristics of solar cells fabricated with AACVD-deposited $CuInS_2$ films.

TABLE II.—*AM*0 OUTPUT CHARACTERISTICS OF SOLAR CELLS FABRICATED WITH *AACVD*-DEPOSITED $CUINS_2$ FILMS

Fabricator	V_{oc} (mV)	I_{sc} (mA/cm^2)	Fill factor	h (percent)
GRC	309	12.5	0.37	1.0
IEC	412	7.2	0.45	1.0

E. Thin Film Deposition of Other Chalcopyrite Materials Using *SSP*s

Throughout the course of research at NASA GRC, *SSP*s for depositing other I-III-VI_2 compounds as thin films have been prepared (refs. 3 and 4). $AgIn_5S_8$ thin films with a thickness of about 1 μm and grain size of approximately 0.5 μm were deposited using a *SSP* which should have afforded bulk $AgInS_2$ (ref. 4). Run to run deposition temperatures were varied between 350 and 450 °C but no changes in crystalline structure were observed, indicating that the deposition temperature was not a limiting factor. $CuGaS_2$ (112)-oriented films were also deposited (ref. 3). These films appeared to be dense with an average grain size of 0.4 μm and bandgap energies of 2.42 eV. An alloy film of $Cu(In:Ga)S_2$ was also deposited using two analogous Ga and In *SSP*s in a dual-source spray *CVD* setup (ref. 3). The deposited film's composition and microstructure varied along the length of the film. The atomic percentage of Ga increased as the length increased. Compositions of $CuIn_{0.43}Ga_{0.57}S_2$, $CuIn_{0.38}Ga_{0.62}S_2$, and $CuIn_{0.27}Ga_{0.73}S_2$ were obtained for the beginning, middle, and end of the film, respectively. The thermal profiles of the two *SSP*s used for depositing these films were unalike. Using two *SSP*s with matching thermal profiles may help in controlling the composition when depositing multi-ternary films.

IV. Conclusion

$CuInS_2$ thin films were grown at low temperatures (<400 °C) via *AACVD* using *SSP*s ($(PPh_3)_2Cu(SEt)_2In(SEt)_2$). During the growth process, it was noticed that (112)-oriented films were close to stoichiometric with no secondary phases present, while (204/220)-oriented films were In-rich and always included an In-rich secondary phase. This indium secondary phase was removed by post-processing annealing at 600 °C, thereby increasing the Cu/In ratio. $CuInS_2$ films grown always exhibited p-type conduction and bandgap energies around 1.46 eV±0.02. Films with a grain size up to 0.5 μm were obtained.

Variation of the deposition zone temperature affected the film stoichiometry and crystalline structure while not significantly affecting the deposition rate. A deposition zone temperature was optimized at 395 °C to produce (112)-oriented films without any detectable secondary phases. The susceptor location within the furnace did not affect the stoichiometry of deposited films but it did alter morphology. Moving the susceptor towards the evaporation zone improved the morphology of the films. Increasing the precursor concentration in the carrier solvent also improved

the morphology of the films while not altering the stoichiometry. *EDS* and XRD analyses indicated that after S-annealing the stoichiometry and crystalline structure of the films was enhanced. *PL* studies revealed four major emission bands (1.45, 1.43, 1.37, and 1.32 eV) together with a broad band associated with deep defects. The blueshift of the 1.45 and 1.37 eV emission bands with increasing excitation power revealed *DAP* transitions. The broad band together with 1.45 and 1.32 eV bands were reduced upon S-annealing due to passivation of V_S.

These films were then further processed to fabricate working solar cells. The best parameters obtained from the cells were the following: the IEC cell had the highest V_{oc} and *FF*, 412 mV and 0.45, respectively, while the GRC cell had the highest I_{sc} with 12.5 mA/cm^2. Devices fabricated at both GRC and IEC showed efficiencies above 1.0 percent (*AM*0). The major challenge has been achieving higher V_{oc}, which seems to be a problem for cells prepared with *AACVD* deposited films in general.

References

1. Banger, K.K., Cowen, J.E., and Hepp, A.F., "Synthesis and Characterization of the First Liquid Single-Source Precursors for the Deposition of Ternary Chalcopyrite ($CuInS_2$) Thin Film Materials," *Chem. Mater.*, vol. 13, no. 11, 2001, pp. 3827–3829.
2. Banger, K.K., Harris, J.D., Cowen, J.E., and Hepp, A.F., "Facile Modulation of Single Source Precursors: the Synthesis and Characterization of Single Source Precursors for Deposition of Ternary Chalcopyrite Materials," *Thin Solid Films*, vols. 403–404, no. 1, 2002, pp. 390–395.
3. Banger, K.K., Hollingsworth, J.A., Harris, J.D., Cowen, J., Buhro, W.E., and Hepp, A.F., "Ternary Single-Source Precursors for Polycrystalline Thin-Film Solar Cells," *Appl. Organomet. Chem.,* vol. 16, no. 11, 2002, pp. 617–627.
4. Banger, K.K., Jin, M.H.-C., Harris, J.D., Fanwick, P.E., and Hepp, A.F., "A New Facile Route for the Preparation of Single-Source Precursors for Bulk, Thin-Film, and Nanocrystallite I-III-VI Semiconductors," *Inorg. Chem.,* vol. 42, no. 24, 2003, pp. 7713–7715.
5. Banger, K.K., Hollingsworth, J.A., Jin, M.H.-C., Harris, J.D., Bohannan, E.W., Switzer, J.A., Buhro, W.E., and Hepp, A.F., "Ternary Precursors for Depositing I-III-VI_2 Thin Films for Solar Cells Via Spray *CVD*," *Thin Solid Films,* vols. 431–432, no. 1, 2003, pp. 63–67.
6. Jin, M.H.-C., Banger, K.K., Kelly, C.V., Scofield, J.H., McNatt, J.S., Dickman, J.E., and Hepp, A.F., "Solar Cells Fabricated with $CuInS_2$ Films Deposited Using Single-Source Precursors," *Proceedings of 19th European Photovoltaic Solar Energy Conference*, WIP, Munich, Germany and ETA, Florence, Italy, 2004, pp. 1943–1946.
7. Jin, M.H.-C., Banger, K.K., Harris, J.D., and Hepp, A.F., "$CuInS_2$ Films Deposited by Aerosol-Assisted Chemical Vapor Deposition Using Ternary Single-Source Precursors," *Mater. Sci. Eng. B*, vol. 116, no. 3, 2005, pp. 395–401.
8. Kelly, C.V., Jin, M.H.-C., Banger, K.K., McNatt, J.S., Dickman, J.E., and Hepp, A.F., "Parametric study on non-vacuum chemical vapor deposition of $CuInS_2$ from a single-source precursor," *Mater. Sci. Eng. B*, vol. 116, no. 3, 2005, pp. 403–408.
9. Jin, M.H.-C., Banger, K.K., McNatt, J.S., Kelly, C.V., Dickman, J.E., and Hepp, A.F., "Post-Deposition Annealing of Thin Film $CuInS_2$ Made from a Single-Source Precursor," *Proceedings of the 31st IEEE Photovoltaic Specialists Conference*, IEEE, Piscataway, NJ, 2005, pp. 382–385.
10. Klaer, J., Bruns, J., Henninger, R., Töpper, K., Klenk, R., Ellmer, K., and Bräunig, D., "A Tolerant Two Step Process for Efficient $CuInS_2$ Solar Cells," *Proceedings of the 2nd World Conference on Photovoltaic Energy Conversion*, Report EUR 18656, vol. I, European Commission, Luxemborg, 1998, pp. 537–540.
11. Ramanathan, K., Contreras, M.A., Perkins, C.L., Asher, S., Hasoon, F.S., Keane, J., Young, D., Romero, M., Metzger, W., Noufi, R., Ward, J. and Duba, A., "Properties of 19.2 percent Efficiency ZnO/CdS/$CuInGaSe_2$ Thin-Film Solar Cells," *Prog. Photovolt. Res. Appl.,* vol. 11, no. 4, 2003, pp. 225–230.
12. Rockett, A. and Birkmire, R.W., "Copper Indium Selenide ($CuInSe_2$) for Photovoltaic Applications," *J. Appl. Phys.,* vol. 70, no. 7, 1991, pp. R81–R97.
13. Bailey, S.G., and Flood, D.J., "Space Photovoltaics," *Prog. Photovolt. Res. Appl.,* vol. 6, no. 1, 1998, pp. 1–14.
14. Schock, H.W. and Noufi, R., "*CIGS*-Based Solar Cells for the Next Millennium," *Prog. Photovolt. Res. Appl.,* vol. 8, no. 1, 2000, pp. 151–160.
15. Archer, M.D. and Hill, R., *Clean Electricity from Photovoltaics*, Imperial College Press, Singapore, 2001, Chapt. 7.
16. Nomura, R., Kanaya, K., and Matsuda, H., "Preparation of Copper Indium Sulfide Thin Films by Solution Pyrolysis of Organometallic Sources," *Chem. Lett.,* vol. 11, no. 12, 1988, pp. 1849–1850.

17. Nomura, R., Fujii, S., Kanaya, K., and Matsuda, H., "Oxygen- or Sulfur-Containing Organoindium Compounds for Precursors of Indium Oxide and Sulfide Thin Films," *Polyhedron,* vol. 9, no. 2–3, 1990, pp. 361–366.
18. Nomura, R., Sekl, Y. and Matsuda, H., "Preparation of Copper Indium Sulfide ($CuInS_2$) Thin Films by Single-Source MOCVD Process Using $Bu_2In(S(i\text{-}Pr))Cu(S_2CN(i\text{-}Pr)_2)$," *J. Mater. Chem.,* vol. 2, no. 7, 1992, pp. 765–766.
19. Nomura, R., Sekl, Y. and Matsuda, H.," Preparation of Copper Indium Sulfide ($CuIn_5S_8$) Thin Films by Single-Source Organometallic Chemical Vapor Deposition," *Thin Solid Films*, vol. 209, no. 2, 1992, pp. 145–147.
20. Hirpo, W., Dhingra, S., Sutorik, A.C., and Kanatzidis, M.G., "Synthesis of Mixed Copper-Indium Chalcogenolates. Single-Source Precursors for the Photovoltaic Materials $CuInQ_2$ (Q = S, Se)," *J. Am. Chem. Soc.* vol. 115, no. 4, 1993, pp. 1597–1599.
21. Hollingsworth, J.A., Hepp, A.F., and Buhro, W.E., "Spray *CVD* of Copper Indium Disulfide Films: Control of Microstructure and Crystallographic Orientation," *Chem. Vap. Deposition,* vol. 5, no. 3, 1999, pp. 105–108.
22. Hollingsworth, J.A., Buhro, W.E., Hepp, A.F., Jenkins, P.P., and Stan, M.A., "Spray Chemical Vapor Deposition of $CuInS_2$ Thin Films for Application in Solar Cell Devices," *Chemical Aspects of Electronic Ceramics Processing*, edited by P.N. Kumta et al., MRS Symposium Proceedings, Volume 495, Materials Research Society, Pittsburgh, PA, 1998, pp. 171–176.
23. Harris, J.D. Hehemann, D.G., Cowen, J.E., Hepp, A.F., Raffaelle, R.P., and Hollingsworth, J.A., "Using Single Source Precursors and Spray Chemical Vapor Deposition to Grow Thin-Film $CuInS_2$," *Proceedings of the 28th IEEE Photovoltaic Specialists Conference*, IEEE, Piscataway, NJ, 2000, pp. 563–566.
24. Krumdieck, S., Sbaizero, O., and Raj, R., "Unique Precursor Delivery and Control Afforded by Low-Pressure Pulsed-*CVD* Process with Ultrasonic Atomization," *J. Phys. IV (Proceedings)*, vol. 11. no. (Proc.) 3, 2001, pp. 1161–1168.
25. Hanket, G., Paulson, P.D., Singh, U., Junker, S.T., Birkmire, R.W., Doyle III, F.J., Eser, E., and Shafarman, W.N., "Fabrication of Graded $Cu(InGa)Se_2$ Films by Inline Evaporation," *Proceedings of the 28th IEEE Photovoltaic Specialists Conference*, IEEE, Piscataway, NJ, 2000, pp. 499–503.
26. Gossla, M., Metzner, H., and Mahnke, H.-E., "$CuInS_2$ Thin-Films from Co-Evaporated Precursors," *Thin Solid Films*, vol. 387, no. 1–2, 2001, pp. 77–79.
27. Töpper, K., Bruns, J., Scheer, R., Weber, M., Weidinger, A., and Braunig, D., "Photoluminescence of $CuInS_2$ Thin Films and Solar Cells Modified by Postdeposition Treatments," *Appl. Phys. Lett.,* vol. 71 no. 4, 1997, pp. 482–484.
28. Jokanovic, V., Janackovic, Dj., Spasic, P., and Uskokovic, D. "Modeling of Nanostructural Design of Ultrafine Mullite Powder Particles Obtained by Ultrasonic Spray Pyrolysis," *Nanostruct. Mater*., vol. 12, no. 1–4, 1999, pp. 349–352.
29. Kodas, T.T. and Hampden-Smith, M.J., *Aerosol Processing of Materials*, Wiley-VCH, New York, 1999, Chapt. 5.
30. M.H.-C. Jin, K.K. Banger, J.D. Harris, J.E. Cowen, A.F. Hepp, "Thin Film $CuInS_2$ Prepared by Spray Pyrolysis with Single-Source Precursors," *Proceedings of the 29th IEEE Photovoltaic Specialists Conference*, IEEE, Piscataway, NJ, 2002, pp. 672–675.
31. Álvarez-García, J., Pérez-Rodríguez, A., Romano-Rodríguez, A., Morante, J.R., Calvo-Barrio, L., Scheer, R., and Klenk, R., "Microstructure and Secondary Phases in Coevaporated $CuInS_2$ Films: Dependence on Growth Temperature and Chemical Composition," *J. Vac. Sci. Technol. A*, vol. 19, no. 1, 2001, pp. 232–239.
32. Weber, M., Scheer, R., Lewerenz, H.J., Jungblut, H., and Störkel, U., "Micro-Roughness and Composition of Cyanide-Treated $CuInS_2$," *J. Electrochem. Soc.*, vol. 149, no. 1, 2002, pp. G77–G84.
33. Look, D.C. and Manthuruthil, J.C., "Electron and Hole Conductivity in Copper Indium Sulfide ($CulnS_2$)," *J. Phys. Chem. Solids,* vol. 37, no. 2, 1976, pp. 173–180.
34. Kazmerski, L.L., Ayyagari, M.S., and Sandborn, G.A., "Copper Indium Sulfide ($CuInS_2$) Thin Films. Preparation and Properties," *J. Appl. Phys.,* vol. 46, no. 11, 1975, pp. 4865–4869.
35. Zhang, S.B., Wei, S.H., Zunger, A. and Katayama-Yoshiba, H., "Defect Physics of the $CuInSe_2$ Chalcopyrite Semiconductor," *Phys. Rev. B*, vol. 57, no. 16, (1998) pp. 9642–9656.
36. Van den Brekel, C.H.J., "Characterization of Chemical Vapor-Deposition Processes. I," *Philips Res. Rep*., vol. 32, no. 2, 1977, pp. 118–133.
37. Siemer, K., Klaer, Luck, I., and Braunig, D., "Influence of Crystal Orientation on Device Performance of $CuInS_2$ Solar Cells," *Proceedings of the 28th IEEE Photovoltaic Specialists Conference*, IEEE, Piscataway, NJ, 2000, pp. 630–633.
38. Siebentritt, S., "Wide gap chalcopyrites: material properties and solar cells," *Thin Solid Films*, vol. 403–404, no. 1., 2002, pp. 1–8.

39. Ueng, H.Y. and Hwang, H.L., "The Defect Structure of Copper Indium Sulfide ($CuInS_2$). Part I. Intrinsic Defects. *J. Phys. Chem. Solids*, vol. 50, no. 12, 1989, pp. 1297–1305.
40. Leite, R.C.C. and DiGiovanni, A.E., "Frequency Shift with Temperature as Evidence for Donor-Acceptor Pair Recombination in Relatively Pure n-Type Gallium Arsenide," *Phys. Rev.*, vol. 153, no. 3, 1967, pp. 841–843.
41. Binsma, J.J.M., Giling, L.J., and Bloem, J., "Luminescence of Copper (I) Indium Sulfide. I. The Broad Band Emission and Its Dependence on the Defect Chemistry," *J. of Luminescence*, vol. 27, no. 1, 1982, pp. 35–53.
42. Binsma, J.J.M., Giling, L.J., and Bloem, J., "Luminescence of Copper (I) Indium Sulfide. II. Exciton and Near Edge Emission," *J. of Luminescence*, vol. 27, no. 1, 1982, pp. 55–72.
43. Ueng, H.Y. and Hwang, H.L., "The Defect Structure of Copper Indium Sulfide ($CuInS_2$). Part II. Thermal Annealing Defects," *J. Phys. Chem. Solids*, vol. 51, no. 1, 1990, pp. 1–10.
44. Schön, J.H. and Bucher, E., "Characterization of Intrinsic Defect Levels in $CuInS_2$," *Phys. Stat. Sol. A*, vol. 171, no. 2, 1999, pp. 511–519.
45. Krustok, J., Raudoja, J., Schön, J.-H., Yakushev, M., and Collan, H., "The Role of Deep Donor-Deep Acceptor Complexes in CIS-Related Compounds," Thin Solid Films, vol. 361–362, no. 1, 2000, pp. 406–410.
46. Nanu, M., Schoonman, J., and Goossens, A., "Raman and *PL* Study of Defect-Ordering in $CuInS_2$ Thin Films," *Thin Solid Films*, vol. 451–452, no. 1, 2004, pp. 193–197.
47. Harris, J.D., Banger, K.K., Scheiman, D.A., Smith, M.A., Jin, M.H.-C., and Hepp, A.F., "Characterization of $CuInS_2$ Films Prepared by Atmospheric Pressure Spray Chemical Vapor Deposition," *Mat. Sci. Eng. B*, vol. 98, no. 2, 2003, pp. 150–155.

REPORT DOCUMENTATION PAGE

Form Approved
OMB No. 0704-0188

1. AGENCY USE ONLY (*Leave blank*)	2. REPORT DATE	3. REPORT TYPE AND DATES COVERED
	November 2006	Technical Memorandum

4. TITLE AND SUBTITLE

Aerosol-Assisted Chemical Vapor Deposited Thin Films for Space Photovoltaics

5. FUNDING NUMBERS

WBS 953033.01.03.23

6. AUTHOR(S)

Aloysius F. Hepp, Jeremiah S. McNatt, John E. Dickman, Michael H.-C. Jin, Kulbinder K. Banger, Christopher V. Kelly, Angel R. Aquino González, and Angus A. Rockett

7. PERFORMING ORGANIZATION NAME(S) AND ADDRESS(ES)

National Aeronautics and Space Administration
John H. Glenn Research Center at Lewis Field
Cleveland, Ohio 44135–3191

8. PERFORMING ORGANIZATION REPORT NUMBER

E–15708

9. SPONSORING/MONITORING AGENCY NAME(S) AND ADDRESS(ES)

National Aeronautics and Space Administration
Washington, DC 20546–0001

10. SPONSORING/MONITORING AGENCY REPORT NUMBER

NASA TM—2006-214445
AIAA–2006–4010

11. SUPPLEMENTARY NOTES

Prepared for the Fourth International Energy Conversion Engineering Conference and Exhibit (IECEC) sponsored by the American Institute of Aeronautics and Astronautics, San Diego, California, June 26–29, 2006. Aloysius F. Hepp, Jeremiah S. McNatt, and John E. Dickman, NASA Glenn Research Center; Michael H.-C. Jin, University of Texas at Arlington, 701 South Nedderman Drive, Arlington, Texas 76019; Kulbinder K. Banger and Christopher V. Kelly, Ohio Aerospace Institute, 22800 Cedar Point Road, Brook Park, Ohio 44142; Angel R. Aquino González and Angus A. Rockett, University of Illinois, 506 S Wright St., Urbana, Illinois 61801. Responsible person, Aloysius F. Hepp, organization code RPV, 216–433–3835.

12a. DISTRIBUTION/AVAILABILITY STATEMENT

Unclassified - Unlimited
Subject Categories: 23 and 44

Available electronically at http://gltrs.grc.nasa.gov
This publication is available from the NASA Center for AeroSpace Information, 301–621–0390.

12b. DISTRIBUTION CODE

13. ABSTRACT ***(Maximum 200 words)***

Copper indium disulfide thin films were deposited via aerosol-assisted chemical vapor deposition using single source precursors. Processing and post-processing parameters were varied in order to modify morphology, stoichiometry, crystallography, electrical properties, and optical properties in order to optimize device-quality material. Growth at atmospheric pressure in a horizontal hot-wall reactor at 395 °C yielded best device films. Placing the susceptor closer to the evaporation zone and flowing a more precursor-rich carrier gas through the reactor yielded shinier, smoother, denser-looking films. Growth of (112)-oriented films yielded more Cu-rich films with fewer secondary phases than growth of (204)/(220)-oriented films. Post-deposition sulfur-vapor annealing enhanced stoichiometry and crystallinity of the films. Photoluminescence studies revealed four major emission bands (1.45, 1.43, 1.37, and 1.32 eV) and a broad band associated with deep defects. The highest device efficiency for an aerosol-assisted chemical vapor deposited cell was 1.03 percent.

14. SUBJECT TERMS

Copper compounds; Photoluminescence; Solar cells; Thin films; Vapor deposition; Pyrolysis

15. NUMBER OF PAGES

23

16. PRICE CODE

17. SECURITY CLASSIFICATION OF REPORT	18. SECURITY CLASSIFICATION OF THIS PAGE	19. SECURITY CLASSIFICATION OF ABSTRACT	20. LIMITATION OF ABSTRACT
Unclassified	Unclassified	Unclassified	